IEEE Access
Multidisciplinary | Rapid Review | Open Access Journal

Received January 29, 2020, accepted February 8, 2020, date of publication February 17, 2020, date of current version March 2, 2020.

Digital Object Identifier 10.1109/ACCESS.2020.2974401

Remaining Useful Life Prediction and State of Health Diagnosis of Lithium-Ion Battery Based on Second-Order Central Difference Particle Filter

YUAN CHEN[1], YIGANG HE[1], ZHONG LI[2], LIPING CHEN[1], AND CHAOLONG ZHANG[3]

[1]School of Electrical Engineering and Automation, Hefei University of Technology, Hefei 230009, China
[2]Anhui Jianghuai Automobile Co., Ltd., Hefei 230092, China
[3]School of Physics and Electronic Engineering, Anqing Normal University, Anqing 246011, China

Corresponding author: Yigang He (18655136887@163.com)

This work was supported in part by the National Natural Science Foundation of China under Grant 51577046 and Grant 51607004, in part by the State Key Program of National Natural Science Foundation of China under Grant 51637004, and in part by the National Key Research and Development Plan (Important Scientific Instruments and Equipment Development) under Grant 2016YFF0102200.

ABSTRACT State of health (SOH) estimation and remaining useful life (RUL) prediction can ensure reliable and safe system operation and reduce unnecessary maintenance costs. In this paper, to improve the accuracy and reliability of SOH estimation and RUL prediction, a novel method based on second-order central difference particle filter (SCDPF) is proposed. By optimizing the importance probability density function, the particle degeneracy phenomenon of particle filter (PF) can be solved. Experiments from the National Aeronautics and Space Administration (NASA) and the Center for Advanced Life Cycle Engineering (CALCE) of the University of Maryland are conducted to demonstrate the effectiveness and satisfactory performance of the proposed SCDPF approach. The maximum error and the root mean square error (RMSE) of the SCDPF fitting approach are quite small, the minimum values of those are 0.006102 Ah and 0.001599, which are lower than those of the unscented particle filter (UPF) and particle filter (PF). The average RUL errors and average PDF width of SCDPF method are also smaller, which validates the accuracy and stability of the proposed method.

INDEX TERMS Second-order central difference particle filter (SCDPF), remaining useful life (RUL), state of health (SOH), lithium-ion battery, particle filter.

I. INTRODUCTION

Prognostics and health management (PHM) is a discipline composed of methods and technologies to evaluate system reliability and safety under actual life cycle conditions to predict fault progression [1]. SOH and RUL, as key approaches of PHM, are estimated to reduce the risk and maintenance costs of battery management system (BMS) [2]. Capacity is chosen as a main health indicator (HI) of SOH estimation, since it plays a significant role in SOC estimation. RUL is defined as the number of cycles remaining from the present cycle to the end of life (EOL) which can be chosen as 70–80% of the nominal capacity. A RUL prediction can be described by the probability distribution function (PDF) of the RUL to show the uncertainty of battery failure.

Model-based and data-driven methods can both be used to predict SOH and RUL. Many data-driven methods have been studied extensively in recent years. Some of these methods are model-free. Incremental capacity analysis (ICA) [3] and differential voltage analysis (DVA) [4] are two kinds of data-driven methods to find mapping from battery features to SOH predictions. ICA and DVA use the normalized incremental capacity peak (IC, $dQ/dV - V$) and the peak of the differential voltage curve (DV, $dV/dQ - Q$), respectively, to estimate the remaining capacity. Artificial neural network (ANN) [5]–[8], support vector machine (SVM) [9], the Box-Cox transformation [10] and the Wiener process [11] are data-driven methods that describe the inherent degradation relationship and trend of the battery by machine learning. Hybrid methods that are combinations of ANN, SVM and other data-driven methods can overcome the limitations of an individual method by better exploiting all available information [12], [13]. Some data-driven methods can extract features from the monitoring data and map them into a degradation model, such as the Gaussian process regression (GPR) model [14], Brownian motion model [15], auto-regressive model [16] and

The associate editor coordinating the review of this manuscript and approving it for publication was Jiajie Fan.

so on. Data-driven methods can obtain an accurate prediction without a deep understanding of electro-chemical principles and an explicit mathematical model. However, a large amount of data is needed for data-driven methods, and their computational complexity is larger.

Model-based methods capture the long-term dependencies of battery degradation based on mathematical aging models. They can be used to predict SOH due to their mathematical simplicity, wide range of validity and good adaptability [17]. A dual exponential model, as mentioned in [18], [19], is most commonly used to represent the capacity degradation trends. The single exponential model and second-order polynomial model [20], which have fewer parameters, can also predict battery capacity degradation, but these models are not as accurate as the dual exponential model. A hybrid model which composed of the Verhulst model and the exponential model is adopted as the empirical degradation model in [21], but this model is complicated.

Model-based methods are often combined with advanced filter techniques, such as the unscented Kalman filter (UKF), the particle filter (PF) [15], and various improved particle filter (PF) algorithms [17], to predict the SOH and RUL of batteries. A particle filter (PF) is a recursive estimator that can be used in nonlinear and non-Gaussian systems based on Bayesian and sequential Monte-Carlo methods with a re-sampling technique. It does not require large amounts of historical data since the data it receives are sequential, making it more suitable for online applications. The samples for the PF are obtained from an importance density function. Since prior probability density is selected as the importance density function and differs greatly from posterior probability density, the samples are not accurate enough. In addition, with increasing iterations, the diversity of the particles is decreases. Then, degradation of the filtering algorithm will be caused. Choosing a reasonable importance density function and re-sampling can address the particle degeneracy phenomenon. Recently, EKF, UKF [22], and support vector regression [23], [24] have been proposed to obtain the importance probability density function. A support vector regression-particle filter (SVR-PF) method is proposed in [24] to improve the standard PF method against the degeneracy phenomenon. Experimental results show that the SVR-PF method has better prediction capability than the PF. Monte Carlo Markov Chain (MCMC) [22], Rao-Blackwellized particle filter (RBPF) [25], and regularized particle filter (RPF) [26] can be used in re-sampling to improve the accuracy of the PF. The Rao-Blackwellized particle filter (RBPF) in [25] is performed to marginalize the probability distribution of state-space sampling over a subspace of the probability distribution of the state. The RBPF is a combination of a PF and a Kalman filter (KF), which is also called a marginalized PF. Experimental results highlight the effectiveness of the proposed RBPF method with a maximum relative error of 6.64%, which is less than the 14.3% error using a PF.

A novel method based on second-order central difference particle filter (SCDPF) is proposed to improve the accuracy of SOH estimation and RUL prediction. Experiments and comparison analysis between PF, UPF, and the proposed SCDPF method are conducted to demonstrate the effectiveness and satisfactory performance of the proposed method.

II. BASIC THEORY

A. PARTICLE FILTER

The particle filter is a recursive estimator based on Bayesian theory. It uses the Monte Carlo method to draw particles from a posterior distribution of the system state- space and assigns a weight to each particle.

A general discrete-time state-space model is needed for the PF to estimate the posterior PDF of the state vector. We establish a dual exponential model to describe the degradation of lithium-ion batteries [18], as shown in (1).

$$Q_k = a \cdot e^{b \cdot k} + c \cdot e^{d \cdot k}, \tag{1}$$

where k is the cycle number, Q_k is the capacity of the battery at cycle k, a and b are parameters which related to the internal impedance, c and d are parameters which related to the aging rate.

The state-space model for a PF can be written as (2).

$$\begin{aligned} x &= f(x_k) = x_{k-1} + \omega_i \\ \omega_i &= \begin{bmatrix} \omega_a & 0 & 0 & 0 \\ 0 & \omega_b & 0 & 0 \\ 0 & 0 & \omega_c & 0 \\ 0 & 0 & 0 & \omega_d \end{bmatrix} \\ y_k &= h(x_k) = x_k(1) \cdot e^{x_k(2) \cdot k} + x_k(3) \cdot e^{x_k(4) \cdot k}, \end{aligned} \tag{2}$$

where $x = (a, b, c, d)$, y_k is the capacity of the battery at cycle k, $N(0, \sigma)$ is Gaussian noise with zero mean, and σ is standard deviation.

The PF algorithm is elaborated in Table 1.

B. THE SECOND-ORDER CENTRAL DIFFERENCE PARTICLE FILTER

The second-order central difference particle filter (SCDPF) and unscented particle filter (UPF) are optimized methods of particle filters using the second-order central difference Kalman filter (SCDKF) and unscented Kalman filter (UKF) respectively as important density functions to solve the problem of the particle degeneracy phenomenon of the PF. The accuracy and stability of the SCDPF and UPF are higher than those of the PF.

The SCDKF is a method to generate a nonlinear distribution by selecting a sampling point. It has a higher theoretical precision than the UKF and is easier to implement. There is no need for the SCDKF algorithm to calculate the Jacobian matrix of the function. The complexity and computational complexity of the algorithm are smaller than those of the UKF. In addition, even if the system is discontinuous and nonlinear, or a singular point exists in it, state estimation can also be performed by SCDKF.

The second-order central difference filter (SCDF) uses the Stirling interpolation formula to expand the nonlinear model

TABLE 1. Procedures of the PF.

Step 1. Initialization: For k=0, randomly generate N particles from the prior Gauss distribution with corresponding particle weights $\{W_0^i\}_{i=1:N}$, where $W_0^{1:N} = 1/N$.

Step 2. Time update: For k=1:N, generate new samples according to $x_k^i \sim q(x_k^i \mid x_{k-1}^i, y_k)$, where $q(x_k^i \mid x_{k-1}^i, y_k)$ is the important density function and y_k is the measured capacity at cycle k. The predicted estimate is $x_k^i = x_{k-1}^i + \omega_i$, $\hat{y}_k^i = h(x_k^i)$, where i=1:N and $\hat{y}_k^i$ is the estimated value of the capacity at cycle k.

Step3. Normalize importance weights: Generate non-normalized importance weights according to $W_k^i = W_{k-1}^i \frac{p(y_k \mid x_k^i) p(x_k^i \mid x_{k-1}^i)}{q(x_k^i \mid x_{k-1}^i, y_k)}$, $W_k^i = (1/\sqrt{2\pi}) \cdot e^{-(y_k - \hat{y}_k^i)^2/2}$.

Normalize weights $W_k^i = W_k^i / \sum_{i=1}^{N} W_k^i$, where i=1:N.

Step4. Re-sampling: The effective sample N_{eff} is calculated as $N_{eff} = 1/\sum_{i=1}^{N} (W_k^i)^2$. If $N_{eff} < \frac{2}{3}N$, the posterior samples can be generated by re-sampling from the current particle set, the corresponding weights are 1/N.

Step5: Output: $\hat{x}_k = \sum_{i=1}^{N} W_k^i x_k^i$.

Step6: RUL prediction:

$Q_{k+L_k^i}^i = a_k^i \cdot e^{b_k^i (k+L_k^i)} + c_k^i \cdot e^{d_k^i \cdot (k+L_k^i)} = Q_{EOL}$, where k is the cycle that the prediction starts from, Q_{EOL} is the capacity at the end of life, and L_k^i is the number of remaining cycles corresponding to Q_{EOL} of each particle.

The estimated PDF of RUL can be approximated by: $P(L_k \mid Q_{0:k}) \approx \sum_{i=1}^{N} W_k^i \delta(L_k - L_k^i)$.

in the form of a central difference. Let $x \in R^n$ be an n-dimensional vector, $y = y(x)$ is expanded at $\bar{x}$ using the Stirling interpolation formula as shown in (3).

$$y \approx f(\bar{x}) + \overline{D}_{\nabla_x} f(\bar{x}) + \frac{1}{2!} \overline{D}_{\nabla_x}^2 f(\bar{x}), \tag{3}$$

where $\overline{D}_{\Delta_x}$ and $\overline{D}_{\Delta_x}^2$ are first-order and second-order difference operators, respectively, as shown in (4).

$$\begin{aligned} \overline{D}_{\Delta_x} f(\bar{x}) &= \frac{1}{\lambda} [\sum_{p=1}^{n} \Delta x_p \mu_p \delta_p] f(\bar{x}) \\ \overline{D}_{\nabla_x}^2 f(\bar{x}) &= \frac{1}{\lambda^2} [\sum_{p=1}^{n} \Delta x_p^2 \delta_p^2 \\ &\quad + \sum_{p=1}^{n} \sum_{\substack{q=1 \\ q \neq p}}^{n} \Delta x_p \Delta x_q (u_p \delta_p)(u_q \delta_q)] f(\bar{x}), \end{aligned} \tag{4}$$

where δ_p is the partial differential operator, μ_p is the mean operator, and λ is the given step size, which can be optimally chosen as $\lambda^2 = 3$.

The SCDKF is described as follows:

Step 1: Generate first-order and second-order mean difference matrix:

Four square root decomposition operators can be obtained by Cholesky decomposition as shown in (5).

$$\begin{aligned} Q &= S_v \times S_v^T, \quad R = S_w \times S_w^T \\ \overline{P} &= \overline{S}_x \times \overline{S}_x^T, \quad \hat{P} = \hat{S}_x \times \hat{S}_x^T, \end{aligned} \tag{5}$$

where Q is the process noise covariance matrix, R is the measuring noise covariance matrix, $\overline{P}$ is the prediction covariance and $\hat{P}$ is the estimated covariance. $\overline{P}$ and $\hat{P}$ are constantly corrected during the filtering process.

The first-order and second-order mean difference matrix for every particle can be defined as in (6) and (7) based on the interpolation approximation formula (3) and the four square root decomposition operators obtained by (5).

$$\begin{aligned} (S_{x\hat{x}}^{(1)}(k))^{(i)} &= \{(f_i(\hat{x}_{k-1} + \lambda \hat{s}_{x,j}, \bar{v}_{k-1}) \\ &\quad - f_i(\hat{x}_{k-1} - \lambda \hat{s}_{x,j}, \bar{v}_{k-1}))/2\lambda\}; \quad j = 1 : n_x \\ (S_{xv}^{(1)}(k))^{(i)} &= \{(f_i(\hat{x}_{k-1}, \bar{v}_{k-1} + \lambda s_{v,j}) \\ &\quad - f_i(\hat{x}_{k-1}, \bar{v}_{k-1} - \lambda s_{v,j}))/2\lambda\}; \quad j = 1 : n_x \\ (S_{y\bar{x}}^{(1)}(k))^{(i)} &= \{(h_i(\bar{x}_k + \lambda \bar{s}_{x,j}, \bar{w}_k) \\ &\quad - h_i(\bar{x}_k - \lambda \bar{s}_{x,j}, \bar{w}_k))/2\lambda\}; \quad j = 1 : n_x \\ (S_{yw}^{(1)}(k))^{(i)} &= \{(h_i(\bar{x}_k, \bar{w}_k + \lambda s_{w,j}) \\ &\quad - h_i(\bar{x}_k, \bar{w}_k - \lambda s_{w,j}))/2\lambda\}; \quad j = 1 : n_v, \end{aligned} \tag{6}$$

$$\begin{aligned} (S_{x\hat{x}}^{(2)}(k))^{(i)} &= \{\frac{(\lambda^2 - 1)^{1/2}}{2\lambda^2} (f_i(\hat{x}_{k-1} + \lambda \hat{s}_{x,j}, \bar{v}_{k-1}) \\ &\quad + f_i(\hat{x}_{k-1} - \lambda \hat{s}_{x,j}, \bar{v}_{k-1}) - 2f_i(\hat{x}_{k-1}, \bar{v}_{k-1}))\}; \\ &\quad j = 1 : n_x \\ (S_{xv}^{(2)}(k))^{(i)} &= \{\frac{(\lambda^2 - 1)^{1/2}}{2\lambda^2} (f_i(\hat{x}_{k-1}, \bar{v}_{k-1} + \lambda s_{v,j}) \\ &\quad + f_i(\hat{x}_{k-1}, \bar{v}_{k-1} - \lambda s_{v,j}) - 2f_i(\hat{x}_{k-1}, \bar{v}_{k-1}))\}; \\ &\quad j = 1 : n_x \\ (S_{y\bar{x}}^{(2)}(k))^{(i)} &= \{\frac{(\lambda^2 - 1)^{1/2}}{2\lambda^2} (h_i(\bar{x}_k + \lambda \bar{s}_{x,j}, \bar{w}_k) \\ &\quad + h_i(\bar{x}_k - \lambda \bar{s}_{x,j}, \bar{w}_k) - 2h_i(\bar{x}_k, \bar{w}_k))\}; \\ &\quad j = 1 : n_x \\ (S_{yw}^{(2)}(k))^{(i)} &= \{\frac{(\lambda^2 - 1)^{1/2}}{2\lambda^2} (h_i(\bar{x}_k, \bar{w}_k + \lambda s_{w,j}) \\ &\quad + h_i(\bar{x}_k, \bar{w}_k - \lambda s_{w,j}) - 2h_i(\bar{x}_k, \bar{w}_k))\}; \\ &\quad j = 1 : n_v, \end{aligned} \tag{7}$$

where $\hat{s}_{x,j}$, $\bar{s}_{x,j}$, $s_{v,j}$, and $s_{w,j}$ represent column j of $\hat{S}_x$, $\bar{S}_x$, S_v, and S_w; $\hat{x}_{k-1}$ and $\bar{x}_{k-1}$ are the system state estimation and prediction at cycle k − 1, respectively; n_x is the dimension of the state vector; and n_v is the dimension of the measurement noise vector.

Step 2: State forecast:

The one-step predictions of the particles are obtained by (8).

$$\begin{aligned} \bar{x}_k^{(i)} &= \frac{\lambda^2 - n_x - n_v}{\lambda^2} f_i(\hat{x}_{k-1}, \bar{v}_{k-1}) \\ &\quad + \frac{1}{2\lambda^2} \sum_{p=1}^{n_v} [f_i(\hat{x}_{k-1}, \bar{v}_{k-1} + \lambda s_{v,p}) + f_i(\hat{x}_{k-1}, \bar{v}_{k-1} - \lambda s_{v,p})] \\ &\quad + \frac{1}{2\lambda^2} \sum_{p=1}^{n_x} [f_i(\hat{x}_{k-1} + \lambda \hat{s}_{x,p}, \bar{v}_{k-1}) + f_i(\hat{x}_{k-1} - \lambda \hat{s}_{x,p}, \bar{v}_{k-1})]. \end{aligned} \tag{8}$$

To obtain the Cholesky factor of the prediction state error mean square matrix, the compound matrix $\overline{S}_x(k)$ is needed as shown in (9).

$$\overline{S}_x^{(i)}(k) = [(S_{x\hat{x}}^{(1)}(k))^{(i)} \ (S_{xv}^{(1)}(k))^{(i)} \ (S_{y\bar{x}}^{(1)}(k))^{(i)} \ (S_{yw}^{(1)}(k))^{(i)}]. \tag{9}$$

QR decomposition is used to transform the rectangular matrix $\overline{S}_x(k)$ into a triangularized square Cholesky factor, which can be calculated by (10).

$$\begin{cases} [Q, R] = qr(\overline{S}_x^{(i)}(k)^T) \\ \overline{S}_x^{(i)}(k) = R. \end{cases} \tag{10}$$

We update the prediction error covariance matrix $\overline{P}_k$ by (11).

$$\overline{P}_k^{(i)} = \overline{S}_x^{(i)}(k)\overline{S}_x^{(i)}(k)^T. \tag{11}$$

The predictive mean square error matrix $\overline{S}_y(k)$ can be calculated using (12).

$$\overline{S}_y^{(i)}(k) = [(S_{y\bar{x}}^{(1)}(k))^{(i)} \ (S_{yw}^{(1)}(k))^{(i)} \ (S_{y\bar{x}}^{(2)}(k))^{(i)} \ (S_{yw}^{(2)}(k))^{(i)}]. \tag{12}$$

According to (13), the Cholesky factor $\overline{S}_y(k)$ can be obtained by the House-holder transform of the compound matrix in a similar way to $\overline{S}_x(k)$.

$$\begin{cases} [Q, R] = qr(\overline{S}_y^{(i)}(k)^T) \\ \overline{S}_y^{(i)}(k) = R. \end{cases} \tag{13}$$

Step 3: State update:

We calculate the predictive measurement capacity $\overline{y}_k$ by (14).

$$\begin{aligned} \overline{y}_k^{(i)} = & \frac{\lambda^2 - n_x - n_w}{\lambda^2} h(\overline{x}_k, \overline{w}_k) \\ & + \frac{1}{2\lambda^2} \sum_{p=1}^{n_x} [h(\overline{x}_k - \lambda \overline{s}_{x,p}, \overline{w}_k) + h(\overline{x}_k + \lambda \overline{s}_{x,p}, \overline{w}_k)] \\ & + \frac{1}{2\lambda^2} \sum_{p=1}^{n_w} [h(\overline{x}_k, \overline{w}_k + \lambda s_{w,p}) + h(\overline{x}_k, \overline{w}_k - \lambda s_{w,p})]. \end{aligned} \tag{14}$$

The cross prediction error mean square matrix $P_{xy}(k)$ can be defined as in (15).

$$P_{xy}^{(i)}(k) = \overline{S}_x^{(i)}(k)[(S_{y\bar{x}}^{(1)}(k))^{(i)}]^T. \tag{15}$$

The Kalman optimal gain K_k can be obtained according to (16).

$$K_k^{(i)} = P_{xy}^{(i)}(k)[S_y^{(i)}(k) \times S_y^{(i)}(k)^T]^{-1}. \tag{16}$$

We update the state estimation $\hat{x}_k$ based on the filter state equation (17).

$$\hat{x}_k^{(i)} = \overline{x}_k^{(i)} + K_k^{(i)}(y_k - \overline{y}_k^{(i)}), \tag{17}$$

where y_k is the actual capacity value.

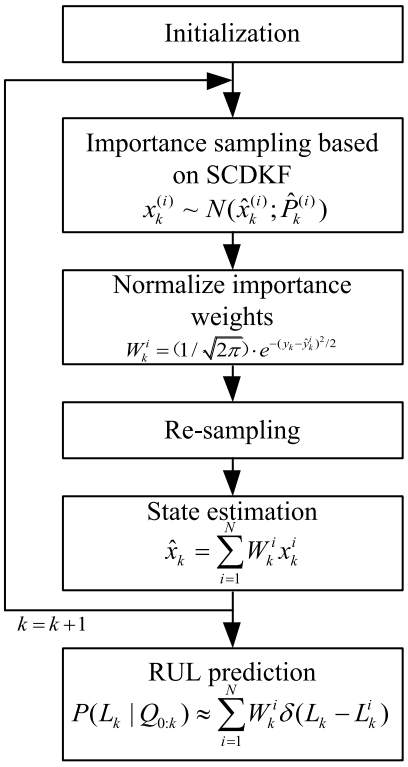

FIGURE 1. A flow chart of SCDPF method.

We calculate the Cholesky factor $\hat{S}_x(k)$, in the same way as $\overline{S}_x(k)$ and $\overline{S}_y(k)$, by (18).

$$\begin{cases} \hat{S}_x^{(i)}(k) = [\bar{S}_x^{(i)}(k) - K_k^{(i)} \ (S_{yx}^{(1)}(k))^{(i)} \ K_k^{(i)} \ (S_{yw}^{(1)}(k))^{(i)} \\ \qquad K_k^{(i)}(S_{yx}^{(2)}(k))^{(i)} \ K_k^{(i)} \ (S_{yw}^{(2)}(k))^{(i)}] \\ [Q, R] = qr(\hat{S}_x^{(i)}(k)^T); \quad \hat{S}_x^{(i)}(k) = R. \end{cases} \tag{18}$$

We update the covariance estimation $\hat{P}_k$ using (19).

$$\hat{P}_k^{(i)} = \hat{S}_x^{(i)}(k)\hat{S}_x^{(i)}(k)^T. \tag{19}$$

The state estimation $\hat{x}_k$ obtained by the SCDKF method is used in importance sampling as shown in (20).

$$x_k^{(i)} \sim N(\hat{x}_k^{(i)}; \hat{P}_k^{(i)}). \tag{20}$$

A complete flow chart is shown in Figure 1 to describe the SCDPF method.

III. EXPERIMENTAL VALIDATION

In this section, two different datasets were used to validate the developed approach. The datasets of type A (A12, A5) were collected from the Center for Advanced Life Cycle Engineering (CALCE) of the University of Maryland and had a rated capacity of 0.9 Ah. By the Arbin BT2000 Battery Test system, the tests were conducted under room temperature. The EOL threshold for capacity fade was set to 80% of the rated capacity [25].

The other datasets of type B (B5, B6) were obtained from the NASA Prognostic Center of Excellence (PCOE). The tests were conducted with a battery prognostics test bed at room temperature, and the batteries were subjected to different

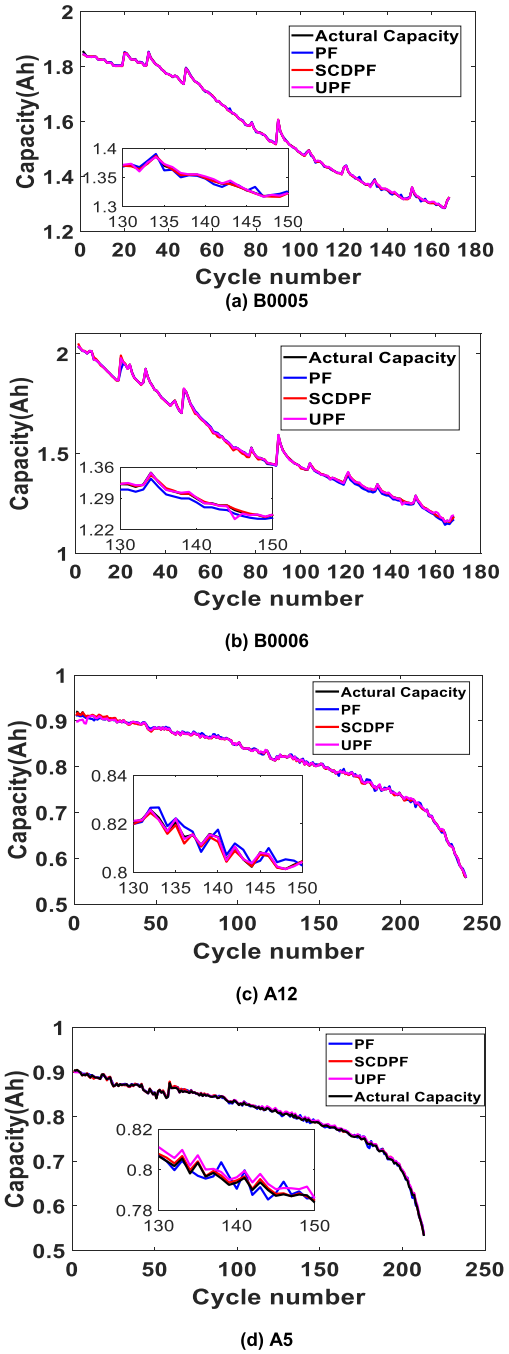

FIGURE 2. The measured and fitted capacity.

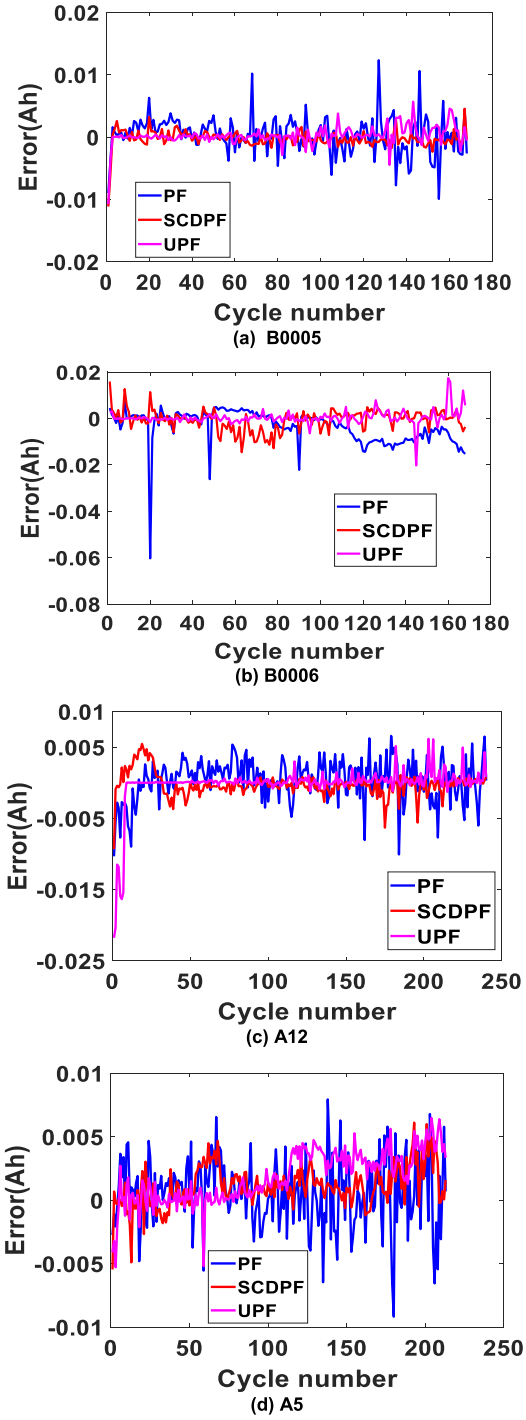

FIGURE 3. Errors of capacity fitting.

conditions, such as charging and discharging. The tests were stopped when EOL was reached [27]. The rated capacity of the two batteries was 2 Ah. The EOL thresholds for datasets B5 and B6 were set to 70% of their initial capacity [22]. Based on the two datasets, the number of particles for the PF method was 500. For the UPF and the proposed SCDPF method, the number of particles was set as 200.

A. CAPACITY ESTIMATION

To compare the accuracy of different methods, the two datasets are used for simulation. The fitted capacity results of the B0005, B0006, A12, and A5 batteries obtained by the PF, UPF, and SCDPF methods are shown in Figure 2. The comparisons of fitted errors are shown in Figure 3.

The capacity comparison between fitted and measured data clearly shows that the conformance is adequate. Apparently, the SCDPF method ensures a better performance with less error compared with the UPF and PF methods, especially for B0005 and B0006. The UPF method is better than the PF method because the error is lower.

TABLE 2. Fitted errors of four cells.

Battery cell	Method	Max error(Ah)	The root mean square error
B0005	PF	0.01232	0.003001
	UPF	0.01176	0.001557
	SCDPF	0.01115	0.001353
B0006	PF	0.0603	0.007284
	UPF	0.02026	0.00309
	SCDPF	0.01593	0.004403
A12	PF	0.01034	0.002898
	UPF	0.02178	0.002993
	SCDPF	0.009326	0.001635
A5	PF	0.09184	0.002711
	UPF	0.006472	0.002029
	SCDPF	0.006102	0.001599

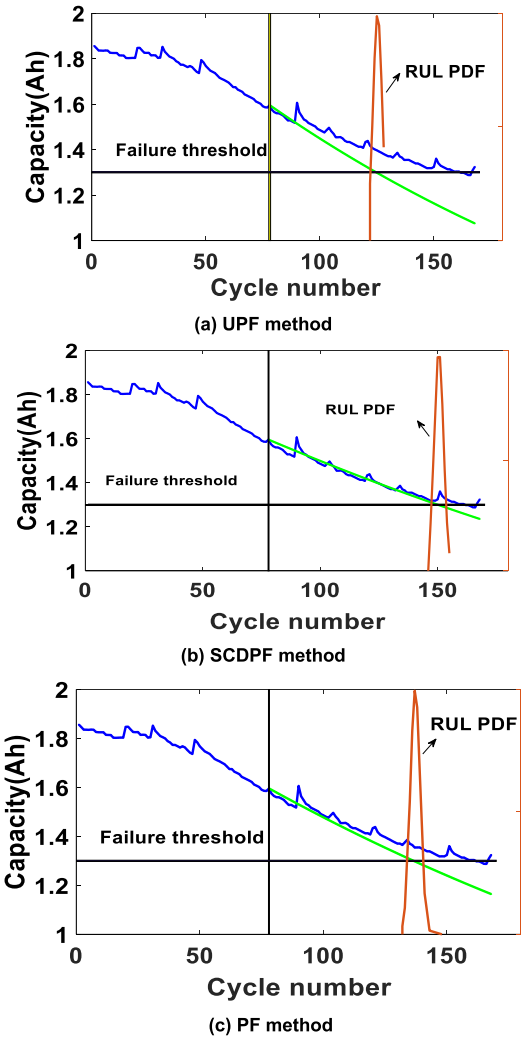

FIGURE 4. SOH and RUL prediction for dataset B0005.

The fitted errors of the four cells are shown in Table 2. The maximum error and the root mean square error (RMSE) of B0005 obtained by the SCDPF fitting approach are 0.01115 Ah and 0.001353, while those obtained by the UPF are 0.01176 Ah and 0.001557, and those obtained by the PF are 0.01232 Ah and 0.003001. Similar results are found

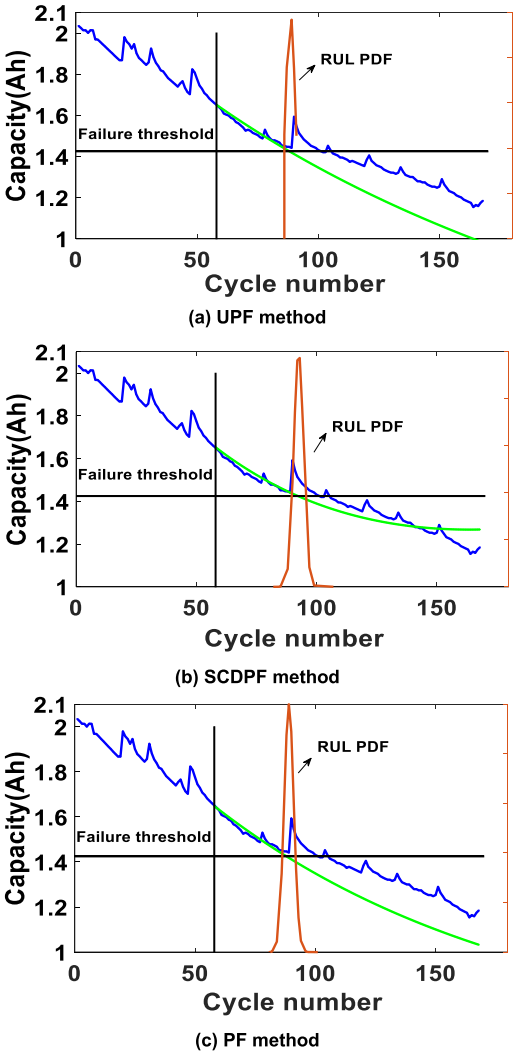

FIGURE 5. Capacity and RUL prediction for dataset B0006.

for batteries B0006, A12, and A5. It can be concluded that the proposed SCDPF fitting approach has a relatively high accuracy as the errors are fewer than those of the other two methods.

B. VERIFICATION OF SOH AND RUL PREDICTION

In this section, the degradation data of cells are utilized to realize the SOH and RUL predictions by using the PF, UPF, and SCDPF methods. SOH and RUL prediction for dataset B0005 with different methods at 78 cycles are shown in Figure 4. The prediction results obtained by the SCDPF method are closer to the true capacity degradation, while the results of the PF method are not as accurate.The maximum value of the RUL PDF for dataset B0005 based on the proposed SCDPF method is also closer to the real RUL. The SOH and RUL predictions for dataset B0006 at 58 cycles are shown in Figure 5. The prediction results and maximum value of the RUL PDF obtained by the SCDPF method are closer to the true value than those obtained by the PF and UPF,

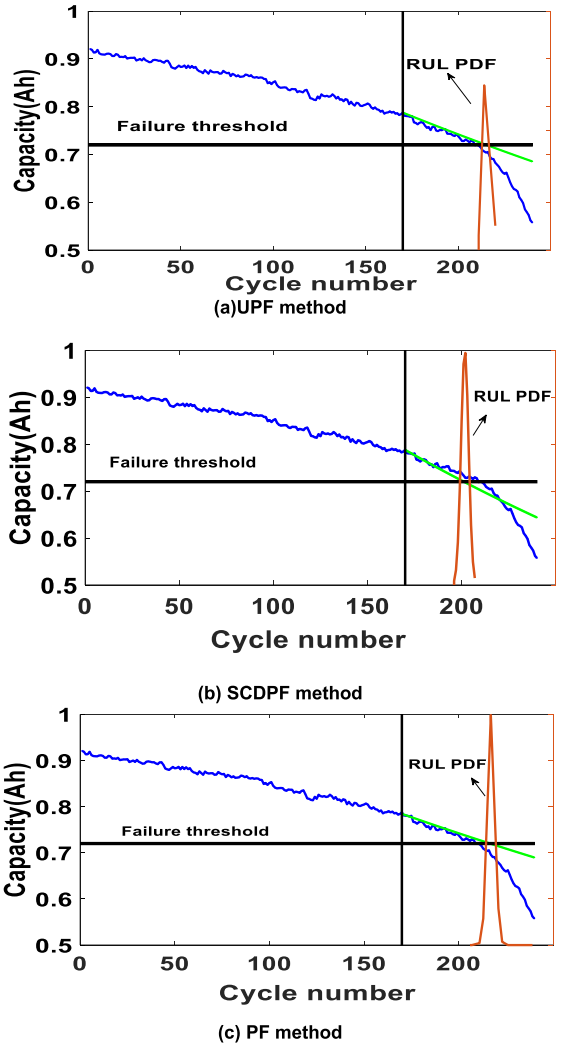

FIGURE 6. SOH and RUL prediction for dataset A12.

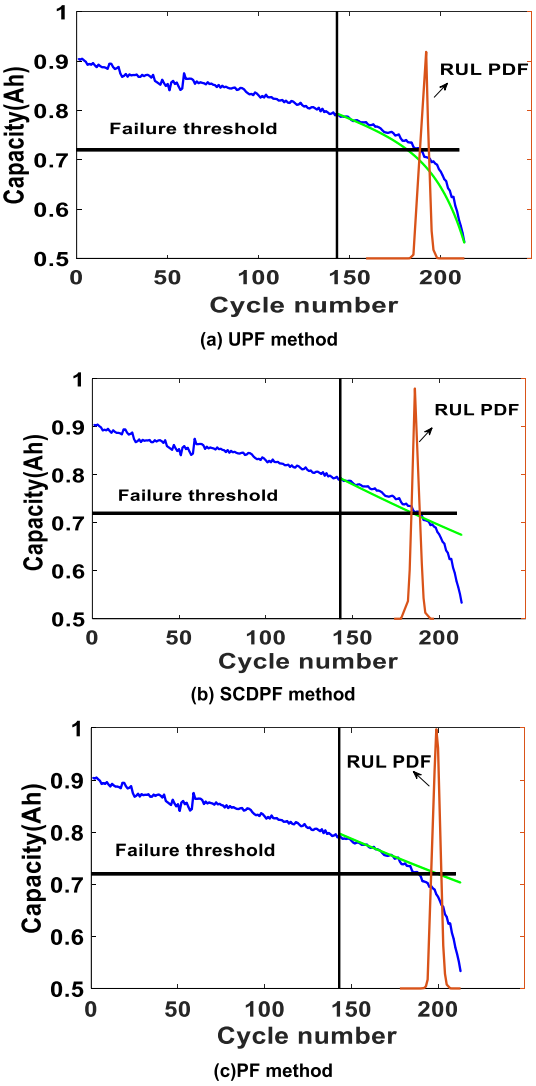

FIGURE 7. SOH and RUL prediction for dataset A5.

which indicates that the prediction accuracy of the proposed SCDPF method is higher. What have to be noticed is that the prediction results and RUL PDF for B0005 obtained by the PF are closer to the true capacity compared to that obtained by the UPF.

Figure 6 and Figure 7 show the SOH and RUL predictions for datasets A12 and A5 using the PF, UPF, and SCDPF methods at cycles 170 and 143, respectively. Similar to datasets B0005 and B0006, the accuracy of the prediction results and the RUL PDF obtained by the proposed SCDPF method is slightly higher than that obtained by the UPF and PF. In contrast to datasets B0005 and B0006, all prediction results and the RUL PDF obtained by the UPF are closer to the true capacity than those obtained by the PF.

Table 3 lists the RUL prediction results of B0005 and B0006 obtained by the three methods. Each method was run 6 times. The average RUL errors of the SCDPF method for B0005 and B0006 are smaller than that of the UPF and PF methods. The errors of the PF for B0005 vary from 8 to 35 and those of the UPF vary from 8 to 35, while those of the SCDPF vary from 9 to 11, which means that the stability of the SCDPF is higher. For the other three cells, the conclusions are similar. Concerning to the uncertainty assessment, it is obvious that the intervals of the proposed SCDPF method have smaller PDF width than those of the PF method for B0005. The PDF width of the UPF method is almost the same as that of the SCDPF method. In addition, the interval of the SCDPF method is closer to the true RUL than that of the PF method. For B0006, the PDF width of the SCDPF method is smaller than that of the PF method but higher than that of the UPF method. Notably, some of the intervals obtained by the proposed SCDPF method can bracket the true RUL precisely, while most of those obtained by the two other methods can not. In general, for B0005 and B0006, the precision and stability of the proposed SCDPF method are higher than those of the other two methods.

The RUL prediction results of A12 and A5 obtained by the PF, UPF, and SCDPF methods are shown in Table 4. The average RUL errors and average PDF width of the SCDPF

TABLE 3. RUL prediction results of B0005 and B0006 for 6 runs.

Method		B0005(Ts=78, RUL=84)				B0006(Ts=58, RUL=43)			
		RUL	Error	Interval	Width	RUL	Error	Interval	Width
PF	1	49	35	41-57	16	37	6	27-49	22
	2	56	28	51-70	19	67	24	37-106	69
	3	68	16	50-83	33	25	18	19-32	13
	4	52	32	47-63	16	65	22	43-95	52
	5	57	27	47-67	20	26	17	22-39	17
	6	76	8	71-83	12	42	1	31-69	38
UPF	1	68	16	62-68	6	38	5	33-40	7
	2	71	13	69-82	13	22	21	20-23	3
	3	59	25	54-59	5	46	3	30-51	21
	4	75	9	72-80	8	24	19	22-24	2
	5	66	18	57-68	11	26	17	25-30	5
	6	75	9	69-81	12	31	12	28-33	5
SCDPF	1	74	10	70-78	8	42	1	29-61	32
	2	73	11	69-79	10	29	14	21-38	17
	3	74	10	68-78	10	38	5	30-55	25
	4	75	9	70-78	8	32	11	21-55	34
	5	73	11	70-77	7	30	13	23-41	18
	6	74	10	71-77	6	34	9	20-41	21

TABLE 4. RUL prediction results of A12 and A5 for 6 runs.

Method		A12(Ts=170, RUL=39)				A5(Ts=143, RUL=45)			
		RUL	Error	Interval	Width	RUL	Error	Interval	Width
PF	1	58	19	41-68	27	57	14	48-69	21
	2	60	21	53-67	14	56	13	42-67	25
	3	70	31	56-70	17	57	13	40-58	18
	4	52	13	43-69	26	54	9	29-68	39
	5	47	8	37-59	22	53	8	28-69	41
	6	54	15	29-70	41	52	7	31-69	38
UPF	1	36	3	25-36	11	56	11	12-69	52
	2	33	6	30-45	15	52	7	35-60	25
	3	57	18	52-66	14	37	8	13-64	51
	4	30	9	22-30	8	27	18	10-69	59
	5	18	21	14-20	6	58	13	26-70	44
	6	17	22	0-70	70	34	11	17-68	51
SCDPF	1	23	16	19-27	8	35	10	29-49	20
	2	26	13	23-29	6	34	11	26-40	14
	3	19	20	17-21	4	60	15	49-69	20
	4	24	15	21-29	8	43	2	31-54	23
	5	32	7	26-37	11	56	11	41-69	28
	6	21	18	18-24	6	34	11	23-44	21

method for A12 and A5 are both smaller than those of the UPF and PF methods, which can lead to the same conclusions as discussed for B0005 and B0006.

IV. CONCLUSION

In this work, a method based on a second-order central difference particle filter (SCDPF) is proposed to predict the SOH and RUL of lithium-ion batteries. Based on a dual exponential model, a second-order central difference Kalman filter is used to obtain the importance probability density function to solve the problem of the degeneracy phenomenon in a PF. As an improvement of the particle filter algorithm, the SCDPF method can perform better than traditional methods. To validate the effectiveness and stability of the proposed method, datasets from NASA and CALCE are applied for SOH and RUL predictions.

The capacity comparison between the fitted and measured data shows that the fitted data obtained by the PF, UPF, and SCDPF methods can all follow the actual capacity value very well, but the SCDPF method has better filtering precision. The maximum error and the root mean square error (RMSE) of the SCDPF fitting approach are quite small, and they are less than those of the UPF and PF methods. For SOH and RUL predictions, the results obtained by the SCDPF method are closer to the true capacity and RUL, which indicates that the accuracy is higher. Concerning the uncertainty assessment, RUL prediction results for 6 runs obtained by the three methods are made. The average RUL errors and PDF width of the SCDPF method are smaller than those of the other methods, confirming that the proposed method is more accurate and stable.

REFERENCES

[1] S. Hong, Z. Zhou, E. Zio, and W. Wang, "An adaptive method for health trend prediction of rotating bearings," *Digit. Signal Process.*, vol. 35, pp. 117–123, Dec. 2014.

[2] R. Xiong, Y. Zhang, J. Wang, H. He, S. Peng, and M. Pecht, "Lithium-ion battery health prognosis based on a real battery management system used in electric vehicles," *IEEE Trans. Veh. Technol.*, vol. 68, no. 5, pp. 4110–4121, May 2019.

[3] J. Tian, R. Xiong, and Q. Yu, "AC model-based incremental capacity analysis for degradation state recognition of lithium-ion batteries," *IEEE Trans. Ind. Electron.*, vol. 66, no. 2, pp. 1576–1584, Feb. 2019.

[4] L. Wang, C. Pan, L. Liu, Y. Cheng, and X. Zhao, "On-board state of health estimation of $LiFePO_4$ battery pack through differential voltage analysis," *Appl. Energy*, vol. 168, pp. 465–472, Apr. 2016.

[5] X. Pang, R. Huang, J. Wen, Y. Shi, J. Jia, and J. Zeng, "A lithium-ion battery RUL prediction method considering the capacity regeneration phenomenon," *Energies*, vol. 12, no. 12, p. 2247, Jun. 2019.

[6] Y. Zhang, R. Xiong, H. He, and M. G. Pecht, "Long short-term memory recurrent neural network for remaining useful life prediction of lithium-ion batteries," *IEEE Trans. Veh. Technol.*, vol. 67, no. 7, pp. 5695–5705, Jul. 2018.

[7] W. Li, Z. Jiao, L. Du, W. Fan, and Y. Zhu, "An indirect RUL prognosis for lithium-ion battery under vibration stress using Elman neural network," *Int. J. Hydrogen Energy*, vol. 44, no. 23, pp. 12270–12276, May 2019.

[8] L. Ren, L. Zhao, S. Hong, S. Zhao, H. Wang, and L. Zhang, "Remaining useful life prediction for lithium-ion battery: A deep learning approach," *IEEE Access*, vol. 6, pp. 50587–50598, 2018.

[9] X. Feng, C. Weng, X. He, X. Han, L. Lu, D. Ren, and M. Ouyang, "Online state-of-Health estimation for li-ion battery using partial charging segment based on support vector machine," *IEEE Trans. Veh. Technol.*, vol. 68, no. 9, pp. 8583–8592, Sep. 2019.

[10] Y. Zhang, R. Xiong, H. He, and M. G. Pecht, "Lithium-ion battery remaining useful life prediction with Box–Cox transformation and Monte Carlo simulation," *IEEE Trans. Ind. Electron.*, vol. 66, no. 2, pp. 1585–1597, Feb. 2019.

[11] S. Tang, C. Yu, X. Wang, X. Guo, and X. Si, "Remaining useful life prediction of lithium-ion batteries based on the wiener process with measurement error," *Energies*, vol. 7, no. 2, pp. 520–547, Jan. 2014.

[12] F. Cadini, C. Sbarufatti, F. Cancelliere, and M. Giglio, "State-of-life prognosis and diagnosis of lithium-ion batteries by data-driven particle filters," *Appl. Energy*, vol. 235, pp. 661–672, Feb. 2019.

[13] L. Zhao, Y. Wang, and J. Cheng, "A hybrid method for remaining useful life estimation of lithium-ion battery with regeneration phenomena," *Appl. Sci.*, vol. 9, no. 9, pp. 1890–1905, May 2019.

[14] D. Yang, X. Zhang, R. Pan, Y. Wang, and Z. Chen, "A novel Gaussian process regression model for state-of-health estimation of lithium-ion battery using charging curve," *J. Power Sources*, vol. 384, pp. 387–395, Apr. 2018.

[15] G. Dong, Z. Chen, J. Wei, and Q. Ling, "Battery health prognosis using brownian motion modeling and particle filtering," *IEEE Trans. Ind. Electron.*, vol. 65, no. 11, pp. 8646–8655, Nov. 2018.

[16] F. Li and J. Xu, "A new prognostics method for state of health estimation of lithium-ion batteries based on a mixture of Gaussian process models and particle filter," *Microelectron. Rel.*, vol. 55, no. 7, pp. 1035–1045, Jun. 2015.
[17] Y. Chang and H. Fang, "A hybrid prognostic method for system degradation based on particle filter and relevance vector machine," *Rel. Eng. Syst. Safety*, vol. 186, pp. 51–63, Jun. 2019.
[18] W. He, N. Williard, M. Osterman, and M. Pecht, "Prognostics of lithium-ion batteries based on Dempster–Shafer theory and the Bayesian Monte Carlo method," *J. Power Sources*, vol. 196, no. 23, pp. 10314–10321, Dec. 2011.
[19] M. V. Micea, L. Ungurean, G. N. Cârstoiu, and V. Groza, "Online state-of-Health assessment for battery management systems," *IEEE Trans. Instrum. Meas.*, vol. 60, no. 6, pp. 1997–2006, Jun. 2011.
[20] Q. Qin, S. Zhao, S. Chen, D. Huang, and J. Liang, "Adaptive and robust prediction for the remaining useful life of electrolytic capacitors," *Microelectron. Rel.*, vol. 87, pp. 64–74, Aug. 2018.
[21] B. Long, W. Xian, L. Jiang, and Z. Liu, "An improved autoregressive model by particle swarm optimization for prognostics of lithium-ion batteries," *Microelectron. Rel.*, vol. 53, no. 6, pp. 821–831, Jun. 2013.
[22] Z. Y. Zhu, "Improved particle filter algorithm based on importance density function selection," in *Particle Filter Algorithm Its Application*, 4nd ed. BeiJing, China: Science Press, 2010, pp. 37–38.
[23] J. Wei, G. Dong, and Z. Chen, "Remaining useful life prediction and state of health diagnosis for lithium-ion batteries using particle filter and support vector regression," *IEEE Trans. Ind. Electron.*, vol. 65, no. 7, pp. 5634–5643, Jul. 2018.
[24] H. Dong, X. Jin, Y. Lou, and C. Wang, "Lithium-ion battery state of health monitoring and remaining useful life prediction based on support vector regression-particle filter," *J. Power Sources*, vol. 271, pp. 114–123, Dec. 2014.
[25] A. El Mejdoubi, H. Chaoui, H. Gualous, P. Van Den Bossche, N. Omar, and J. Van Mierlo, "Lithium-ion batteries health prognosis considering aging conditions," *IEEE Trans. Power Electron.*, vol. 34, no. 7, pp. 6834–6844, Jul. 2019.
[26] C. Musso, N. Oudjane, and F. Le Gland, "Improving regularised particle filters in Sequential Monte Carlo Methods," in *Practice*. New York, NY, USA: Springer, 2001.
[27] B. Saha and K. Goebel. *Battery Data Set, NASA AMES Prognostics Data Repository*. Accessed: 2007. [Online]. Available: http://ti.arc.nasa.gov/project/prognostic-datarepository

YUAN CHEN received the B.Sc. and M.Sc. degrees from the China University of Mining and Technology, in 2010 and 2012, respectively. She is currently pursuing the Ph.D. degree with the School of Electrical and Automation Engineering, Hefei University of Technology. Her current research interests include prediction and fault diagnosis of the battery management systems.

YIGANG HE received the M.Sc. degree from Hunan University, in 1992, and the Ph.D. degree from Xi'an Jiaotong University, in 1996. From 2011 to 2017, he worked as the Head of the School of Electrical Engineering and Automation, Hefei University of Technology. He is currently working as the Vice-Head of the School of Electrical Engineering and Automation, Wuhan University. His current research interests include testing, and fault diagnosis of circuits and smart grid.

ZHONG LI received the bachelor's degree from the China University of Mining and Technology, Xuzhou, China, in 2012. He is currently working as an Engineer with the JAC Automotive Technology Center. His current research interests include prediction and fault diagnosis of the battery management systems.

LIPING CHEN received the B.S. degree in applied mathematics from Anhui Normal University, Wuhu, China, in 2007, and the Ph.D. degree in control theory and control engineering from Chongqing University, Chongqing, China, in 2013. He is currently an Associate Professor with the Hefei University of Technology, Hefei, China. His current research interests include fractional-order systems, nonlinear dynamical systems, and battery management systems.

CHAOLONG ZHANG received the Ph.D. degree from the Hefei University of Technology, Hefei, China, in 2018. He is currently a Postdoctoral Researcher with the Electrical Engineering and Automation, Wuhan University, Wuhan, China. He is also an Associate Professor with the School of Physics and Electronic Engineering, Anqing Normal University, Anqing, China. His current research interests include fault diagnostics and prognostics of analog and mixed-signal circuits, and battery capacity prognostic.